ACS OMEGA

http://pubs.acs.org/journal/acsodf

Article

Electron Tunneling in Biology: When Does it Matter?

Setare Mostajabi Sarhangi and Dmitry V. Matyushov*

Cite This: *ACS Omega* 2023, 8, 27355−27365

Read Online

ACCESS | Metrics & More | Article Recommendations | Supporting Information

ABSTRACT: Electrons can tunnel between cofactor molecules positioned along biological electron transport chains up to a distance of ≃ 20 Å on the millisecond time scale of enzymatic turnover. This tunneling range determines the design of biological energy chains facilitating the cross-membrane transport of electrons. Tunneling distance and cofactors' redox potentials become the main physical parameters affecting the rate of electron transport. In addition, universal charge-transport properties are assigned to all proteins, making protein identity, flexibility, and dynamics insignificant. This paradigm is challenged by dynamical models of electron transfer, showing that the electron hopping rate is constant within the crossover distance $R^* \simeq 12$ Å, followed with an exponential falloff at longer distances. If this hypothesis is fully confirmed, natural and man-made energy chains for electron transport should be best designed by placing redox cofactors near the crossover distance R^*. Protein flexibility and dynamics affect the magnitude of the maximum hopping rate within the crossover distance. Changes in protein flexibility between forward and backward transitions contribute to vectorial charge transport. For biological energy chains, charge transport through proteins is not defined by universal parameters, and protein identity matters.

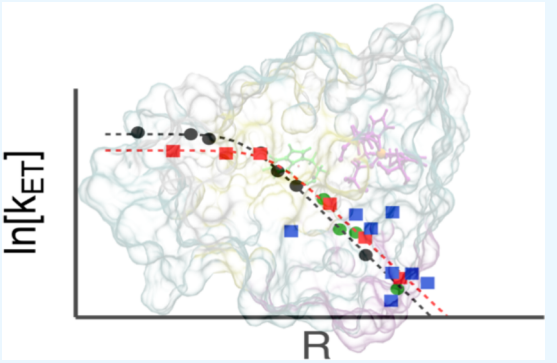

INTRODUCTION

Experimental studies of tunneling in biology were initiated by a 1966 paper by DeVault and Chance.[1] They reported the kinetics of oxidation of cytochrome proteins by photoexcited reaction centers of photosynthetic bacterium *Chromatium*. The half-time of the reaction was found to increase from ≃ 2 μs at room temperature to ≃ 2.3 ms at 100 K and stayed nearly constant down to 35 K (Figure 1). The fast component of the reaction dynamics followed Arrhenius kinetics, but the slow decay was found to be "very nearly if not actually temperature independent".[1] Tunneling was proposed to explain observations, and that set in motion an extensive research program to study tunneling and, more generally, quantum effects in biology.[2]

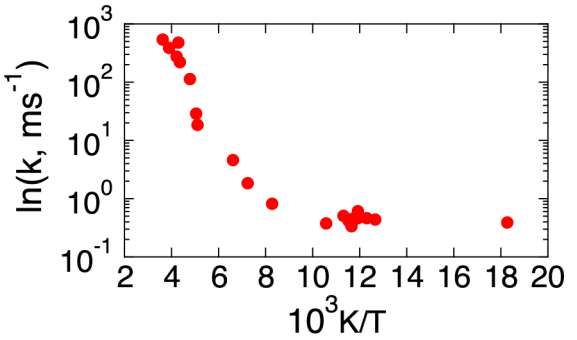

Figure 1. Rate constant for cytochrome oxidation by photoexcited reaction center of the photosynthetic bacterium *Chromatium*.[1] The activation barrier is nearly zero at $T < 100$ K as explained by prevalence of tunneling. Adapted with permission from D. DeVault and B. Chance, Studies of Photosynthesis Using a Pulsed Laser I. Temperature Dependence of Cytochrome Oxidation Rate in Chromatium. Evidence for Tunneling, Biophys J. **1966** 6, 825. Copyright 1966 by Elsevier.

Tunneling is presently an accepted view to explain transport of two subatomic particles responsible for all energy of life: the electron and the proton.[2] The cross-membrane separation of electrons and protons is the basis of Mitchell's chemiosmotic hypothesis.[3,4] The question that has haunted several generations of scientists is whether transport of charges occurs as a coherent process, through conduction bands,[5−7] or through multiple decoherent tunneling hops between sites of charge localization. Despite a number of suggestions of coherent transport through biopolymers,[8−10] the prevailing view is that intraprotein charge transport occurs through decoherent hops between redox cofactors intercalated in the protein fold.[11,12] Proteins can also polymerize in nanowires to deliver electrons over micrometer distances in the process called extracellular electron transfer.[13,14] However, in that case

Received: April 20, 2023
Accepted: July 11, 2023
Published: July 20, 2023

ACS Publications

© 2023 The Authors. Published by American Chemical Society

as well, the prevailing conductivity mechanism is thought to be incoherent hops between sites of electron localization.[15−17]

Electron tunneling between localized states follows Gamow's prescription[18] of under-barrier transition between two unperturbed stationary eigenstates at the opposite sides of the tunneling barrier. If the energies of quantum states involved in tunneling are equal, the probability of penetrating the barrier scales exponentially, $\propto \exp[-\gamma R]$, with the barrier width R often viewed as the edge-to-edge distance between the molecules involved.[19] This exponential falloff of the tunneling probability is retained in the so-called electronic coupling promoting electronic radiationless transitions (without a photon involved[20])

$$V(R) \propto \exp\left[-\frac{1}{2}\gamma R\right] \tag{1}$$

where γ is the inverse tunneling decay distance.

The electronic coupling is the perturbation of the electronic Hamiltonian that brings about electronic transitions between electronic states spatially localized at the donor and acceptor. It defines the rate constant for nonadiabatic (NA) electronic transitions according to Fermi's golden rule equation[21]

$$k_{NA} = \frac{2\pi}{\hbar}\langle V(R)^2 \delta(X)\rangle \tag{2}$$

The rate constant k_{NA} describes the single-exponential decay of the donor population after the transition has been initiated. This is typically achieved by photoexcitation,[22] as was realized by photoexciting the reaction center's primary pair in the DeVault and Chance experiments.[1]

The reaction coordinate X in eq 2 was introduced by Lax[20] and later by Warshel[23] as the collective coordinate monitoring the progress of a radiationless transition. Given that resonance of the initial and final energies is required for tunneling, X is defined as the difference (energy gap) between the final, $E_2(\mathbf{q})$, and initial, $E_1(\mathbf{q})$, energies specified on the manifold $\mathbf{q}$ of the medium's nuclear degrees of freedom

$$X(\mathbf{q}) = E_2(\mathbf{q}) - E_1(\mathbf{q}) \tag{3}$$

The delta-function $\delta(X)$ in eq 2 imposes the condition $X(\mathbf{q}) = 0$ of tunneling resonance.

The average $\langle \cdots \rangle$ in eq 2 is taken over the statistical configurations of nuclear coordinates $\mathbf{q}$. The donor−acceptor distance R is a part of this manifold and can fluctuate as a result of thermal agitation.[9,24] If the donor−acceptor complex is sufficiently rigid, one can separate the equilibrium electronic coupling V_e at the equilibrium donor−acceptor distance R_e from fluctuations of the coupling due to distance changes $\delta R = R - R_e$. One therefore finds that the rate constant is proportional to V_e^2 and exponentially decays with the equilibrium distance

$$k_{NA} \propto V_e^2 \propto e^{-\gamma R_e} \tag{4}$$

Alternatively, when fluctuations of the coupling are significant, as is the case with azurin electron transfer, one defines

$$V_e^2 = \langle V(R)^2\rangle \tag{5}$$

at $R_e = \langle R\rangle$.

A significant body of experimental work went into studies of the distance decay of k_{NA}. Specifically, Winkler and Gray introduced the technique of attaching a photoexcitable Ru^{II} complex to the surface of a redox-active protein. By varying the attachment site, an impressive range of donor−acceptor distances was sampled[12,25,26] (Figure 2). These studies have

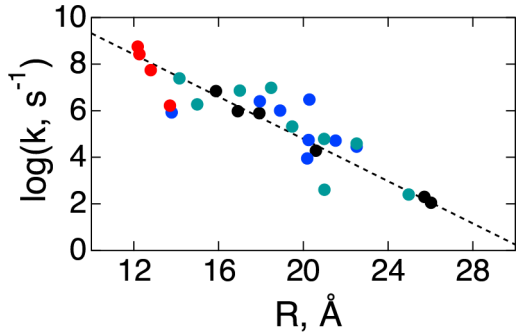

Figure 2. Rate constants of activationless electron transfer vs the donor−acceptor distance for Ru-modified proteins: azurin (black), cytochrome c (blue), cytochrome c-b562 (cyan), and high-potential iron protein (red).[26] The dashed black line is drawn through the azurin data with an exponential decay constant of 1.04 Å^{-1}. The experimental results (points) are adapted with permission from H. B. Gray and J. R. Winkler, Natural engineering principles of electron tunneling in biological oxidation−reduction, *Chem. Sci.* **2021**, 12, 13988. Copyright 2021 by Royal Society of Chemistry.

resulted in an average value of $\gamma \simeq 1.1-1.2$ Å^{-1} assigned to protein media. A similar value, $\gamma \simeq 1.4$ Å^{-1}, was extracted from studies of kinetics of photosynthetic reactions[27,28] (Figure 3).

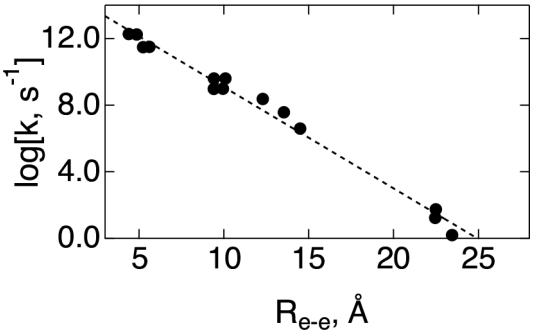

Figure 3. Rate constants of electron transfer in photosynthetic reaction centers vs the edge-to-edge distance $R_{e\text{-}e}$ between the redox cofactors (points).[11] The rate constants are recalculated to the values of the zero activation barrier. The dashed line is the linear fit through the point with the slope γ = 1.4 Å^{-1}. The plot is adopted with permission from C. C. Moser et al., Nature of biological electron transfer, Nature **1992**, 355, 796. Copyright 1992 by Nature.

The available data allow a significant simplification of the theory of protein electron transfer[28] in terms of electronic coupling and the activation barrier $\Delta F^{\dagger}$. The activation barrier is obtained by taking the statistical average of the delta-function in eq 2 in the framework of Marcus theory[29] leading to an analytical formula for the nonadiabatic rate constant

$$k_{NA} \propto V_e^2 e^{-\beta \Delta F^{\dagger}} \tag{6}$$

Here, $\beta = (k_B T)^{-1}$ is the inverse temperature, and the activation barrier $\Delta F^{\dagger}$ is specified in Marcus theory by two parameters, the reaction free energy ΔF_0 and the reorganization energy λ

https://doi.org/10.1021/acsomega.3c02719
ACS Omega 2023, 8, 27355−27365

$$\Delta F^{\dagger} = \frac{(\lambda + \Delta F_0)^2}{4\lambda} \quad (7)$$

A "universal" value of the reorganization energy $\lambda \simeq 0.8$ eV is typically assigned to protein electron transfer.[27]

The combination of eqs 6 and 7 offers a universal picture of protein electron transfer. Both the tunneling decay parameter γ and the reorganization energy λ are viewed as parameters generic to protein media. The only parameters left to tune the reaction rate are the donor−acceptor distance and the reaction free energy. This picture also suggests that the closest packing of cofactors allowed by steric constraints is the best strategy to maximize molecular/protein conductivity.[16,30] Such close packing is not required in biological energy chains, where the limiting factor is the catalytic turnover rate,[27] leading to the donor−acceptor distance $R = R_D \simeq 12-15$ Å (Dutton radius) for reactions with near zero reaction free energy ($\Delta F_0 \simeq 0$). This distance can be extended to $\simeq 21$ Å for activationless transitions[26] ($-\Delta F_0 = \lambda$ in eq 7).

The universal, based on the golden rule (eq 2) view of protein electron transfer comes in stark contrast to many early and modern ideas advocated to explain the catalytic effect of enzymes. An early explanation of the catalytic effect is due to Pauling,[31] who suggested that enzymes preferentially stabilize the reaction activated state, thus reducing the barrier. This view is clearly inconsistent with the theory of nonadiabatic electron transfer operating in terms of equilibrium free energies (λ and ΔF_0) and does not involve any notion of the transition-state configuration and its stabilization by the protein. A more recent suggestion incorporates nonstatistical, dynamical aspects of protein flexibility[32] as a potential reason for the catalytic effect.[33−35] It is nevertheless obvious that none of these concepts have entered the present formulation of the theory of protein electron transfer. The present-day universal theory does not involve individual properties of a specific protein, such as dynamics, elasticity, conformational flexibility, etc. The formalism discussed here aims to change this view.

We offer a formalism that incorporates protein elasticity into the rate of electron transfer in the form of elastic modulation of the tunneling probability. The calculations performed here suggest that most intraprotein electron-transfer reactions are controlled by the medium dynamics and not by the tunneling probability. Tunneling becomes important only at distances exceeding the crossover distance R^*, at which the dynamical control of the rate constant is switched to the tunneling control. Therefore, no reaction speedup can be achieved by placing redox cofactors at distances closer than the crossover distance, and optimal rate of electron transport is achieved when cofactors are placed at separations close to R^*.

The demand to develop a framework alternative to the theory of nonadiabatic electron transfer (eqs 6 and 7) came from a somewhat unexpected direction. Advances in electrochemistry of redox species attached to monolayers self-assembled at the metal electrode[36] have led to the development of thin-film electrochemistry of redox-active proteins.[37−40] This technique provides the dependence of the electrochemical rate constant on the thickness of the monolayer, i.e., on the tunneling distance.[41−44] While the value $\gamma \simeq 1$ Å^{-1} from solution studies (Figures 2 and 3) was confirmed by electrochemical measurements (Figure 4), unexpected results have also emerged.

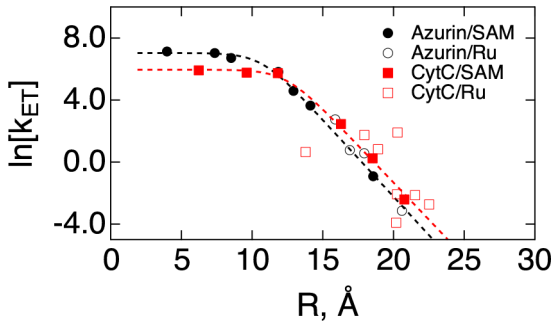

Figure 4. Apparent rate constants of electron transfer between a metal electrode and different proteins immobilized on SAMs of varying thickness: azurin (black) and cytochrome c on CO_2^--terminated SAMs (CytC, red). The dashed lines are fits to eq 9 assuming an exponential falloff of the electronic coupling (eq 4). The open points (Azurin/Ru and CytC/Ru) are taken from solution measurements in Figure 2 and vertically shifted to align with the electrochemical data. Note a very good agreement in the distance decay between electrochemical and solution measurements for azurin. The experimental results are reproduced with permission from[26,45] H. B. Gray and J. R. Winkler, Natural engineering principles of electron tunneling in biological oxidation−reduction, *Chem. Sci.* **2021**, 12, 13988. Copyright 2021 by Royal Society of Chemistry; D. Alvares-Paggi et al., The role of protein dynamics and thermal fluctuations in regulating cytochrome c/cytochrome c oxidase electron transfer, Biochim. Biophys. Acta - Bioenergetics **2014**, 1837, 1196. Copyright 2014 by Elsevier.

First, it was discovered that the rate constant saturates to a plateau at distances $R < R^* \simeq 12-15$ Å. Surprisingly, one finds that the crossover distance falls close to the Dutton radius

$$R_D \simeq R^* \quad (8)$$

Second, the reorganization energies measured by electrochemistry are consistently below the "universal" value of 0.8 eV, falling in the range 0.2−0.5 eV. The first observation is explained by the dynamical control of electron transfer.[46−50] This general formulation yields the rate constant of electron transfer k_{ET} as the ratio of the nonadiabatic, golden rule expression (eq 2) and the correction factor $1 + g$

$$k_{ET} = (1 + g)^{-1} k_{NA} \quad (9)$$

Importantly, the crossover parameter

$$g \propto \tau_X V_e^2 \quad (10)$$

in eq 9 is proportional to the product of the squared electronic coupling V_e^2 and the relaxation time τ_X of $X(t)$ supplied experimentally or computationally by the Stokes-shift dynamics.[51,52] Therefore, with decreasing the donor−acceptor distance and thus increasing the electronic coupling V_e, one arrives at the crossover condition $g(R^*) = 1$. At $R < R^*$, the squared electronic coupling V_e^2 cancels out from the numerator and denominator in eq 9, and the rate constant switches from the nonadiabatic, distance-dependent function to the limit of Kramers kinetics[53−55]

$$k_{ET} \propto \tau_X^{-1} \quad (11)$$

The rate constant reaches a plateau and does not depend on electronic coupling anymore (Figure 4).

Even though measurements seem to be qualitatively consistent with the view of the dynamical control of electron transfer, an attempt to fit the data to the standard model[46−50]

https://doi.org/10.1021/acsomega.3c02719
ACS Omega 2023, 8, 27355−27365

has produced the Stokes-shift relaxation time $\tau_X \simeq 200$ ns,[38] which is much higher than anticipated either from solution measurements[56] or from molecular dynamics simulations of the half redox reaction of cytochrome *c*.[57] The mystery was resolved by allowing fluctuations of the donor−acceptor distance,[44,58] producing a new time scale

$$\tau_\gamma = (\gamma^2 D_R)^{-1} \tag{12}$$

This is the time required for the redox-active protein to diffuse through the tunneling decay distance γ^{-1} with the translational diffusion constant D_R. The time τ_γ competes with τ_X for the dynamical control of the reaction rate, but, even more importantly, the Stokes-shift relaxation time becomes modified with a factor carrying the information about the protein elasticity in the form of the variance of the donor−acceptor distance $\sigma_R^2 = \langle(\delta R)^2\rangle$

$$\tau_X \rightarrow \tau_{\text{eff}} = \tau_X \exp\left[\frac{3}{2}\gamma^2\langle(\delta R)^2\rangle\right] \tag{13}$$

Protein flexibility enters the theory through both the dynamics of the donor−acceptor distance and its statistical variance. The effective time entering the dynamical crossover parameter g becomes longer for media allowing donor−acceptor flexibility, thus increasing the crossover distance R^*.

As mentioned above (eq 8), the crossover length, $R^* \simeq 12$−15 Å,[45] nearly coincides with the maximum distance $\simeq 14$−15 Å within which most activated electron-transfer reactions are found in biological energy chains.[26,59] If R^* found by electrochemistry can be extended to intraprotein electron transfer, that would imply that most intraprotein electron-transfer hops occur in the limit of dynamical control when tunneling does not affect the rate. Experiments by DeVault and Chance, discussed at the beginning of this section, apply to interprotein electron transfer and might still be controlled by tunneling. However, one faces a number of significant questions, including the issue of the magnitude and temperature dependence of the Stokes-shift relaxation time. Given that the relaxation time becomes slower with lowering temperature, the crossover distance R^*, $g(R^*) = 1$ is expected to grow with cooling (eq 10). Therefore, even if interprotein electron transfer is controlled by tunneling at high temperatures, it might fall under the umbrella of dynamical control with cooling.

The present article extends our previous results[60] for intraprotein electron transfer between tryptophan (Trp) residue of azurin and its active site to a single-residue mutation replacing tryptophan with tyrosine (Tyr, Figure 5). The reaction of transferring the hole from Trp to Cu^I of the active site was studied experimentally by Shih et al.,[61] and the reaction time of $\tau_{ET} \simeq 31$ ns was reported. Trp−Tyr mutation was also attempted but resulted in no observable transition. Our calculations confirm a significant rate constant drop upon mutation.

The hole on Tyr is experimentally created by photoexcitation of a Re^I-diimine complex attached to the protein surface and labeled A* in the following reaction scheme

$$\begin{aligned}(0)\ A^* - \text{Tyr} - Cu^I \rightarrow (1)\ A^- - \text{Tyr}^+ - Cu^I \\ \xrightarrow{k_{ET}} A^- - \text{Tyr} - Cu^{II}\ (2)\end{aligned} \tag{14}$$

The cation radical Tyr^+ is produced in less than 1 ps, followed with electron transfer from the active site of azurin to Tyr^+.

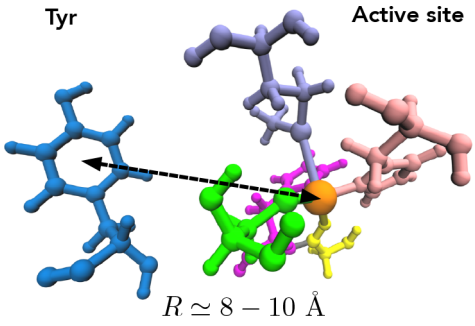

Figure 5. Drawing of the Cu-ligated active site and the tyrosine (Tyr) residue of azurin (PDB 1AZU). The distance between Cu and the center of mass of the phenol ring of Tyr is $R_e = 8.5$ Å for the neutral Tyr state and 9.7 Å for the cation radical state Tyr^+.

This is the reaction studied here by combining the analytical dynamical theory of electron transfer[62] with classical molecular dynamics (MD) simulations.

The tyrosine cation radical Tyr^+ is unstable in the aqueous solution and is expected to lose a phenolic proton also in the protein environment.[63] We therefore additionally studied the reaction of electron transfer from the azurin active site to deprotonated neutral tyrosyl radical $Tyr^\bullet$

$$(1)\ \text{Tyr}^\bullet - Cu^I \xrightarrow{k_{ET}} \text{Tyr}^{\bullet -} - Cu^{II}\ (2) \tag{15}$$

This reaction channel assumes that deprotonation occurs faster than electron transfer in the mechanism shown in eq 14.

RESULTS

Dynamical Theory of Protein Electron Transfer. The dynamical formulation of the theory of protein electron transfer is complicated by the fact that a number of competing nuclear modes, relaxing on similar time scales, affect the reaction dynamics near the crossing point of the free energy surfaces along the reaction coordinate X. The crossing point specifies the activation barrier, and the competing time scales enter the dynamical crossover parameter g in eq 9. The most significant nuclear modes competing in the pre-exponential factor of the rate constant are the medium polarization and the donor−acceptor distance. The dynamics of these two nuclear modes are coupled in the parameter g given by the following equation[62]

$$g = \frac{2\pi V_e^2 \tau_X}{\hbar\sigma_X} \frac{e^{3\gamma^2\langle(\delta R)^2\rangle/2}}{\sqrt{2\beta\Delta F^\ddagger + 4(\tau_X/\tau_R)\gamma^2\langle(\delta R)^2\rangle}} \tag{16}$$

Here, $\sigma_X^2 = 2\lambda k_B T$ is the variance of the electron-transfer energy gap from polarization fluctuations. All parameters in eq 16, except for γ, depend on the electron transfer state $i = 1$ and 2; this dependence is dropped for brevity. We discuss the magnitude of g for the charge-transfer reaction $1 \rightarrow 2$ shown in eqs 14 and 15. The simulation protocol for producing trajectories $X(t)$ and $R(t)$ follows our previous study of wild type azurin and is described in the Supporting Information (SI). Here, we focus on the results.

The crossover parameter in eq 16 depends on the Stokes-shift relaxation time τ_X and the relaxation time of the donor−acceptor dynamics τ_R. Both are calculated as average (integral) relaxation times from the corresponding normalized time correlation functions

https://doi.org/10.1021/acsomega.3c02719
ACS Omega 2023, 8, 27355−27365

Table 1. Reorganization Energies and Activation Barriers (eV) for the Forward and Backward Transitions in the Charge Shift Reactions in eqs 14 and 14 at T = 300 K

State	λ	λ^{St}	$\Delta F^{\dagger}$	τ_X[a]	τ_R	$\langle R\rangle$[b]	R^*	$\langle(\delta R)^2\rangle$[b]	g[c]	τ_{ET}[d]
$Tyr^+ - Cu^I$	1.03	1.30	0.02	8.5	18.3	9.7	10.8	0.09	9	0.047
$Tyr - Cu^{II}$	2.01		1.05	10.4	58.0	8.5	10.8	0.42	62	
$Tyr^{\bullet} - Cu^I$	1.11	1.63	0.23	75.6	72.8	9.8	11.4	0.10	20	445
$Tyr^{\bullet -} - Cu^{II}$	2.23		0.57	42.7	41.9	8.9	13.7	0.93	4814	

[a]Relaxation times (ps) for the Stokes-shift dynamics τ_X and for the donor−acceptor distance τ_R. [b]The average donor−acceptor distance (Å) and its variance (Å^2). [c]The dynamical crossover parameter (eq 16). [d]$\tau_{ET} = k_{ET}^{-1}$ in ns; backward reactions are much slower, $\tau_{ET} \simeq 3$ s for eq 15.

$$S_Y^{(i)}(t) = \frac{\langle \delta Y(t)\delta Y(0)\rangle_i}{\langle (\delta Y(0))^2\rangle_i} \tag{17}$$

where the variable $Y(t)$ is either $X(t)$ or $R(t)$ and $\delta Y(t) = Y(t) - \langle Y\rangle_i$; $\langle \cdots \rangle_i$ specifies an ensemble average in two different electron-transfer states i = 1, 2 (eqs 14 and 15). These calculations (SI) show that electrostatic interactions and the donor−acceptor distance relax on comparable time scales (Table 1).

Another significant parameter is the protein flexibility expressed in terms of the donor−acceptor distance variance $\sigma_{R,i}^2 = \langle(\delta R)^2\rangle_i$ (Table 1). The average distance between tyrosine's phenol ring and the Cu atom of the active site $\langle R\rangle_i$ changes somewhat between the two states, but the main structural difference between the two electron-transfer states is in the distance variance. Consistent with our previous simulations of wild type azurin,[60] the state with a higher number of water molecules around the residue shows a greater distance flexibility. In the present simulations, a larger number of water molecules was found around neutral Tyr (Figure S17), which is reflected by a broader distribution of donor−acceptor distances (Figures S5 and S6) and a larger distance variance (Table 1). It appears that better hydrated active sites are also more flexible.

For the dynamic parameters listed in Table 1 and $\Delta F^{\dagger} \simeq 0.02$ eV calculated below, we find that the first term under the square root in the denominator of eq 16 dominates over the second term. The crossover parameter can be simplified in this case to the following expression in which only the Stokes-shift relaxation time enters the crossover parameter

$$g = \frac{\pi V_e^2}{\hbar\sqrt{\lambda \Delta F^{\dagger}}}\tau_{eff} \tag{18}$$

where τ_{eff} is given by eq 13, and g enters the rate constant pre-exponential factor according to eq 9. The rate constant is in the dynamics-controlled plateau region (Figure 6) at $g > 1$ and $R < R^*$.

Q-Model of Protein Electron Transfer. Calculating the free energy barrier for electron transfer requires constructing the free energy surfaces of electron transfer corresponding to the initial, $F_1(X)$, and final, $F_2(X)$, states. The standard approach[29] is to produce crossing Marcus parabolas with the activation barrier given by eq 7. This approach is, however, not applicable to the energetics of electron transfer in azurin.

The two electron-transfer states in eq 14 are characterized by different wetting patterns of the Tyr residue (Figure S17). The consequence of this new physics is that the reorganization energy from the energy gap variance becomes state-dependent (Table 1)

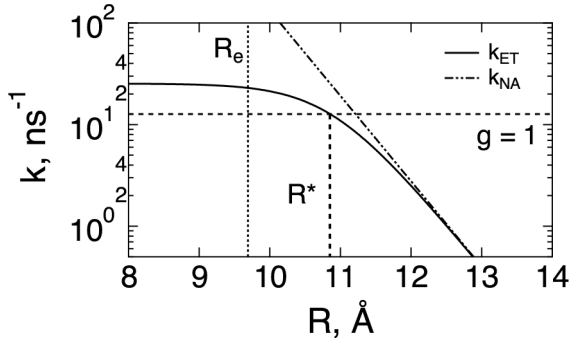

Figure 6. Rate constant of 1 → 2 electron transfer (eq 14) vs the distance between the Cu atom of the active site and the center of mass of the tyrosine phenol ring (Figure 5). The calculated nonadiabatic rate constant k_{NA} (eq 6, dashed-dotted line) is compared to the full electron-transfer rate constant k_{ET} (eq 9, solid line). The horizontal dashed line shows $g(R^*) = 1$, $R^* = 10.9$ Å, and the vertical dotted line indicates the equilibrium distance $R_e = \langle R\rangle_1 = 9.7$ Å from MD trajectories.

$$\lambda_i = \frac{1}{2}\beta\langle(\delta X)^2\rangle_i \tag{19}$$

These two values of the variance reorganization energy are also different from the Stokes-shift reorganization energy[64]

$$2\lambda^{St} = X_1 - X_2 \tag{20}$$

where $X_i = \langle X\rangle_i$ are two average values of the energy gap calculated from trajectories in equilibrium with the corresponding electron-transfer state i = 1, 2. In Marcus theory, all three reorganization energies are equal: $\lambda^{St} = \lambda_1 = \lambda_2$. Their inequality demands an extension to nonparabolic free-energy surfaces delivered here by the Q-model of electron transfer.[65] This model stipulates the following inequality between three reorganization energies

$$\lambda_1 < \lambda^{St} < \lambda_2 \tag{21}$$

where λ_1 and λ_2 can be swapped to match a given reaction. The main requirement for the model to be mapped on a specific physical situation is that the Stokes-shift reorganization energy falls between two variance reorganization energies.

The Q-model is based on three independent parameters: any two reorganization energies out of λ_i, and λ^{St} can be used along with the experimental reaction free energy ΔF_0 to construct $F_i(X)$ (see SI for details). The reaction free energy ΔF_0 for the reaction in eq 14 requires the reduction potentials of azurin, equal to E^0 = 0.341 V,[66] and of $Tyr^+/Tyr^{\bullet}$. The radical cation tyrosine is unstable and loses its phenolic proton in solution to give the neutral tyrosyl radical $Tyr^{\bullet}$. The formal potential of $Tyr^{\bullet}$ is 1.0 V against NHE. The potential for the cation radical has been estimated as 1.38 V in water and even higher, ≃ 1.8−

https://doi.org/10.1021/acsomega.3c02719
ACS Omega 2023, 8, 27355−27365

1.9 V, in a dehydrated, low-dielectric protein environment.[67] The reaction free energy for the reaction in eq 14 thus changes between $\Delta F_0 = -1.04$ eV in the former case and $\Delta F_0 = -1.46$ eV in the latter.

Combining the Q-model parameters for the reaction in eq 14, one arrives at nonparabolic free energy surfaces shown in Figure 7. The lower portion of each surface, shown by points,

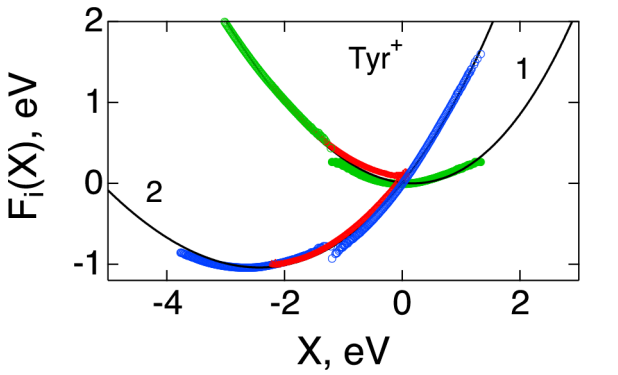

Figure 7. Free energy surfaces of electron transfer for reduction of tyrosine cation radical (eq 14) calculated from the Q-model (solid lines; see SI) and compared to MD simulations (points). The lower points are from simulations of the 1 and 2 states in the reaction scheme in eq 14. The upper portions of the simulation data are obtained from the results around the minima by applying the linear relation from eq 22. Red points are from simulations in the intermediate state with $z = 1/2$ according to eq 23. The calculations are based on the estimated value of the reaction free energy, $\Delta F_0 = -1.04$ eV. (Figure S15 presents the results with $\Delta F_0 = -1.46$ eV).

is calculated directly from sampling the energy gap (eq 3) on the MD simulation trajectories. In contrast, the upper portions are obtained from the linear relations to which $F_i(X)$ satisfy[23,68−70] if the statistics of the medium follows from the Gibbs ensemble[71]

$$F_2(X) = F_1(X) + X \tag{22}$$

Even though the surfaces $F_i(X)$ are nonparabolic, eq 22 is exactly satisfied by the Q-model.

The solid lines in Figure 7 are produced with the Q-model, which is in good agreement with the simulation data. The main result of these calculations is that the forward reaction in the reaction scheme shown in eq 14 is essentially activationless, with the activation barrier of $\Delta F^{\dagger} \simeq 17$ meV. This result is not significantly modified if the reduction potential of 1.8 V, leading to $\Delta F_0 = -1.46$ eV, is adopted for $Trp^+/Trp^{\bullet}$ reduction in a dehydrated protein medium. The reaction shifts to the inverted region in this case, resulting in an even smaller activation barrier of $\Delta F^{\dagger} \simeq 5$ meV (Figure S15).

We have additionally applied the umbrella sampling technique[69,72,73] and simulated the system in the state halfway between the initial and final states and characterized by the Hamiltonian $H_z = H_1 + z(H_2 - H_1)$ (see SI). The corresponding free energy surface is

$$F_z(X) = F_1(X) + zX \tag{23}$$

which becomes $F_1(X)$ at $z = 0$ and $F_2(X)$ at $z = 1$. The simulation was performed at $z = 1/2$. The red points in Figure 7 show $F_1(X) = F_{1/2}(X) - X/2$ and $F_2(X) = F_{1/2}(X) + X/2$.

The reduction potential of $Tyr^{\bullet}/Tyr^{\bullet-}$ is 0.68 V, and the reaction free energy for electron transfer becomes $\Delta F_0 = -0.34$ eV. The free energy surfaces are calculated for the reaction mechanism in eq 15 from the reorganization energies listed in Table 1 by applying the Q-model and are compared to direct sampling of MD trajectories in Figure 8. The activation barrier is significantly increased to $\Delta F^{\dagger} \simeq 0.23$ eV in this case, making the electron-transfer reaction much slower, as we discuss next.

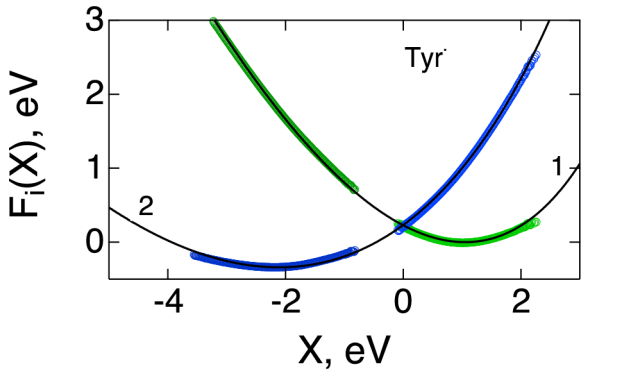

Figure 8. Free energy surfaces for reduction of deprotonated $Tyr^{\bullet}$ (eq 15) calculated from the Q-model (solid lines; see SI) and compared to MD simulations (points). The lower points are from simulations of the 1 and 2 states in the reaction scheme in eq 15. The upper portions of the simulation data are obtained from the results around the minima by applying the linear relation from eq 22. The calculations are based on the estimated value of the reaction free energy $\Delta F_0 = -0.34$ eV.

Electronic Coupling and Rate Constants. The rate constants of electron transfer were calculated from eq 9 by including the nonadiabatic rate constant k_{NA} and the dynamic crossover parameter g in eq 9. The rate constant k_{NA} was calculated as elsewhere[60] by adopting V_e (eq 6) as provided by Voityuk[74] (see SI)

$$\log_{10} V_e(R) = 1.73 - 0.42(R/\text{Å}) \tag{24}$$

This calculation yields the reaction time $\tau_{NA} = k_{NA}^{-1} = 4.6$ ps for the cationic Tyr (eq 14) and a much longer reaction time of 21 ns for the tyrosyl radical (eq 15). Accounting for the dynamic crossover parameter g in eq 9 leads to $\tau_{ET} = k_{ET}^{-1} \simeq 47$ ps in eq 14 and 445 ns in eq 15. The reaction time for the nearly activationless reaction involving Tyr^+ is similar to $\simeq 40$ ps reported for electron-transfer activationless quenching of photoexcited Trp by heme of myoglobin ($R \simeq 12$ Å),[75] but is much shorter than $\tau_{ET} \simeq 31$ ns reported[61] for the reaction involving Trp residue in wild type azurin. No reaction was reported for the Tyr-substituted azurin mutant,[61] and it seems quite likely that Tyr^+ loses its phenolic proton, switching to a much slower reaction path involving the deprotonated tyrosyl radical (eq 15). If this mechanism is adopted, the present rate calculations are in agreement with measurements.[61]

The electronic coupling given by eq 24 is consistent with many ab initio calculations of electronic coupling,[76−78] placing it in the range $V_e \simeq 1-10$ meV for the donor−acceptor distances studied here.[79] Figure 9 compares Voityuk's equation with recent calculations of electronic coupling between heme cofactors in filamentous outer-membrane cytochrome type S proteins.[80] On the other hand, recent time-dependent DFT calculations of hole injection to azurin[81] produced much higher, 50−100 meV, electronic coupling between the Re

https://doi.org/10.1021/acsomega.3c02719
ACS Omega 2023, 8, 27355−27365

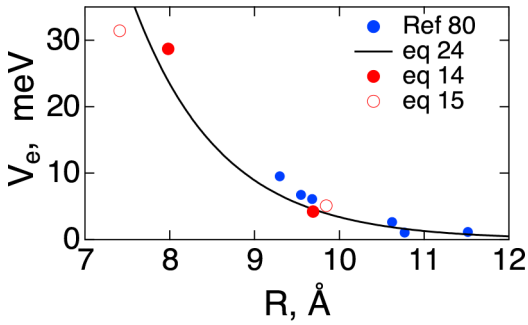

Figure 9. V_e vs the center-to-center donor−acceptor distance from ref 80 compared to the Voityuk equation (solid line, eq 24).[74] The red points indicate the results of the present calculations (eq 5, see SI) for protonated (filled points, eq 14) and deprotonated (open points, eq 15) Tyr.

complex (A* in eq 14) and the Trp residue of azurin placing the reaction step 0 → 1 in eq 14 to the domain of adiabatic electron transfer.[82] In contrast, electron transfer discussed here (second step, 1 → 2, in eq 14) is a nonadiabatic reaction controlled by medium dynamics.[46−50] The rate constants in both regimes, adiabatic and medium-controlled nonadiabatic, do not depend on electronic coupling.

To justify the use of eq 24, we calculated $V(R)$ between Tyr and the active site of azurin both in a vacuum and in the protein (see SI). The value of coupling in the protein is highly fluctuating between different protein configurations.[9,24] Given that the standard deviation is of the same order of magnitude as the average, the mean value is not well-defined, and eq 5 was used to estimate V_e at $R_e = \langle R \rangle$. These results are shown by the red points in Figure 9. A good agreement with eq 24 justifies its use to produce the distance dependence of the rate constant (Figure 6).

The variance of the donor−acceptor distance turns out to be much larger for the oxidized state of the active site for both reaction mechanisms (Table 1). This change in the distance variance, implying a more flexible protein structure, leads to a substantial increase in the effective relaxation time (eq 13) and a corresponding increase in the dynamical parameter g in the rate constant in eq 9. Given that all forward and backward reactions studied here fall in the dynamics-controlled regime of electron transfer, $g > 1$, the backward transitions are slowed down not only by their corresponding activation barriers but also by the rate constant pre-exponential factors scaling in this case as g^{-1}. Asymmetry between forward and backward charge transfer, contributing to unidirectional charge flow, has both thermodynamic and dynamic origins.

A small activation barrier found here for the protonated Tyr^+ and for the wild-type Trp residue in our previous calculations[60] is consistent with nearly temperature-independent rates observed for wild-type azurin:[83] the rate constant is unaffected by temperature between 220 and 300 K and even increases when the temperature is lowered to 170 K. The barrier can shift to lower values with lowering temperature due to protein compression affecting the component of X_i arising from induction interactions of the transferring electron with the electronically polarizable medium.[64] Conductivity of the entire azurin in a solid-state junction (with no hydration water) is temperature-independent down to 4 K.[84] Charge transfer between Trp and the active site is the rate-determining step in the delivery of the hole to the protein surface[61] in a sequence of steps with reaction times τ_i. Given that the overall rate is $k = (\sum_i \tau_i)^{-1}$, the activationless character of the rate-determining step might explain the overall independence of azurin's conductivity of temperature. Note that the rate becomes temperature-dependent above ∼200 K when Cu is replaced by other metals or removed from azurin.[85,86] This result can be caused by an alteration of ΔF_0 resulting in a higher activation barrier.

The reduction of Tyr^+ occurs on the fast time scale of 40−50 ps and can potentially compete with deprotonation of Tyr^+ losing its phenolic proton.[63] Fast electron transfer, however, refers to the hydrated configuration of the Tyr pocket, which is accomplished on the time scale of ≃ 150 ns (Figure S16). Given that electron transfer to the deprotonated tyrosyl radical $Tyr^\bullet$ is about 10^4 times slower, the competition between the rate of wetting/deprotonation and the rate of direct electron transfer becomes essential given that tyrosines are viewed as elements of chains of aromatic residues transporting oxidizing electron holes to avoid oxidative damage to enzymes' active sites.[16,26,61,87−89]

Limitations and Empirical Evidence. The main result of our simulations and calculations is that the electron transfer in azurin is dynamically controlled. We find $g \gg 1$ (Table 1), significantly reducing the rate constant compared to the values anticipated by standard nonadiabatic theories of protein electron transfer (eq 6). Electronic tunneling does not affect the rate in this limit, and the rate constant is instead affected by the protein identity (dynamics and flexibility).

One wonders if empirical evidence supports this picture. Protein thin-film electrochemistry (Figure 4) provides strong support, but there are no complementary data collected for reactions in solution. The distance decay of azurin reaction rates is highly consistent between electrochemical and solution experiments (open and closed circles in Figure 4). However, the solution measurements do not reach the turning point at $R \simeq R^*$, falling short of confirming the dynamical control of protein electron transfer. Alternative evidence comes from the kinetic isotope effect when electron-transfer rates in normal and heavy water are compared. There is no theoretical reason for water deuteration to affect the activation barrier within the classical Marcus picture of crossing parabolas.[90] Nevertheless, a number of recent reports have demonstrated a substantial effect of deuteration on the rate of protein electron transfer.[17,41,91] This kinetic isotope effect can be attributed to altering dynamics of the protein upon deuteration for reactions controlled by dynamics ($g > 1$ in eq 9).[92] The existence of an unexpectedly strong kinetic isotope effect is an indication that these reactions fall into the regime of dynamical control.

In addition to persisting uncertainties with electronic coupling (see SI), calculations of the reaction barrier suffer from their own difficulties. The atomistic simulations used to sample the reaction coordinate $X(t)$ are carried out with nonpolarizable force fields. Corrections for the medium electronic polarizability often require scaling the reorganization energies down by a factor of ≃ 0.8.[70,76,93,94] Our estimates for the activation barrier likely provide an upper bound of the true value, but these uncertainties do not affect the crossover distance R^*.

DISCUSSION

Returning to DeVault and Chance experiments, theoretical interpretations of their data by Hopfield[95] and Jortner[96] have

https://doi.org/10.1021/acsomega.3c02719
ACS Omega 2023, 8, 27355−27365

shown that the change in the Arrhenius slope at low temperatures comes from the quantum nature of nuclear modes coupled to electron transfer. The corresponding temperature plateau of the reaction rate (the lower-temperature part in Figure 1) reflects nuclear tunneling of collective normal-mode vibrations (in contrast to localized, single particle atomic tunneling[97]). The picture following from this analysis, and the shape of the rate temperature dependence, are consistent with kinetic data reported by Frauenfelder and coworkers for a quite different process: migration of CO in hemoglobin[98] and cytochrome *c*.[99] In both systems, similarly to electron transfer rates in Figure 1, one observes a low-temperature plateau attributed to nuclear tunneling (Figure 10). Therefore, it is not electron tunneling that is responsible

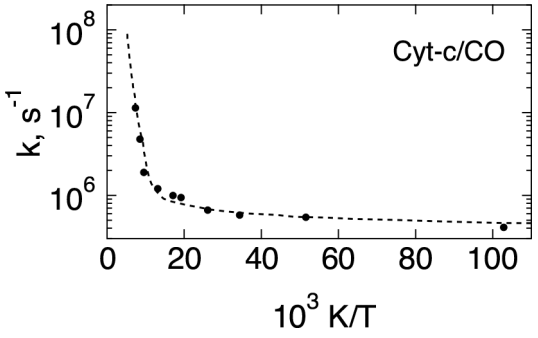

Figure 10. Rate constant for the binding of CO to cytochrome *c* as a function of temperature. The dashed line is a fit through the experimental data points[99] adopted with permission from H. Frauenfelder, Molecular tunneling in heme proteins, In: Tunneling in Biological Systems, Eds. B. Chance and D. DeVault and H. Frauenfelder and R. A. Marcus and J. R. Schrieffer and N. Sutin. Copyright 1979 Academic Press.

for the change in the temperature slope in the Arrhenius plot. Electron tunneling occurs at all temperatures, and it is only the statistics of nuclear fluctuations that change with temperature, allowing nuclear tunneling to occur at low temperatures.

Is it only the statistics of fluctuations that matters? Quoting from Szent-Gyorgyi, "The fuel of life is the electron, or, more exactly, the energy it takes over from photons in photosynthesis; this energy the electron gives up gradually when flowing through the cellular machinery".[100] To do so, electrons must tunnel between localized states in the absence of conduction bands in disordered molecular systems. Tunneling occurs at all temperatures relevant to biology, but the overall transition probability is also affected by the dynamics of barrier crossing, as established already by the Landau–Zener model of nonadiabatic transitions.[21,54] The dynamics of transversing the region where Born–Oppenheimer electronic terms cross must enter the description at some point.

Medium dynamics near the tunneling configuration compete with the tunneling time $\simeq \hbar/V_e$ (not to be confused with the time spent by the particle to tunnel through the barrier[101]). The overall observable rate reflects the slowest rate-determining step in a complex kinetic scheme. It is expressed mathematically in terms of the dynamical crossover parameter *g* in the pre-exponential factor of the rate constant (eq 9). Even though the rate of tunneling accelerates at shorter donor–acceptor distances, the slower processes of friction-driven barrier crossing start to dominate in the overall rate of population decay. It is not that tunneling does not exist anymore, but it is not reflected in the reaction rate constant, which enters the plateau region at shorter donor–acceptor separations. This is the domain of Kramers' kinetics[53−55] when the relaxation time determines the rate constant's pre-exponential factor. This point was expressed by an early insight from Frauenfelder and Wolynes:[54] "...friction and steric effects may play a far more important role in proteins than in simpler systems". For electron transfer, friction dominates in the range of donor–acceptor separations $R < R^*$. It is in this range where protein dynamics and flexibility start to affect the rate.

The observation that rates of protein electron hops are not given by universal parameters applicable to all proteins[27,28] and are, instead, affected by protein identities resonates with a general idea, advocated recently,[32] that dynamical aspects can affect rates of enzymatic reactions.[33−35] The existing electron-transfer theories do not allow such dynamic effects for either biological proton or electron transfer, since protein dynamics do not enter standard formulations. The picture of dynamical effect on electron transfer allows a departure from this tradition, at least in a limited range of distances $R < R^*$ where the reaction is affected by protein flexibility. Given that the effective relaxation time scales exponentially with the variance of the donor–acceptor distance (eq 13), flexible media must show more propensity for electron transport affected by dynamics. Importantly, this observation suggests a new design principle for biological energy chains: no reaction speedup can be achieved by placing redox cofactors at distances closer than R^*. This new principle demands a new understanding of the conductivity through stacked residues and cofactors in biomolecules. For instance, conducting bacterial nanowires[102] are made of stacked pairs of cytochrome *c* proteins[17,103] with the edge-to-edge distances of 3.4–4.1 within one pair and 5.4–6.1 Å between pairs. Whether these systems are flexible enough to allow $R_e < R^*$ remains an open question. Azurin itself is viewed as an exceptionally stable and rigid protein[104] raising the question of whether lifting the level of the distance-independent plateau in Figure 6 through rigidity is a general principle of operation for charge-transfer proteins.

In his groundbreaking paper[3] outlining the chemiosmotic theory of oxidative phosphorylation, Mitchell noted that "it represents the result of carrying to its logical conclusion the present trend towards recognizing the equivalent status of supramolecular and molecular features in channeling of chemical processes in living organisms". Theories of electron transfer developed in recent decades have placed their main focus on the "molecular" aspects of the problem when supramolecular features of the protein–water and protein–membrane–water media do not show up. The protein itself, in this view, only helps to hold the cofactors in sufficiently rigid active sites but otherwise produces little effect on electron-transfer kinetics. The present focus brings the "supramolecular" component of the problem back to light. Proteins allow catalytic lowering of the activation barrier,[71,105] but also affect the rate constant's pre-exponential factor through protein dynamics (τ_X and τ_R) and protein flexibility ($\langle\langle(\delta R)^2\rangle\rangle$).

CONCLUSIONS

Electrons can tunnel between cofactors of biological energy chains to up to $\simeq$ 21 Å on the millisecond time scale of enzymatic turnover. This tunneling range mostly determines the design principles of biological charge-transfer chains made

https://doi.org/10.1021/acsomega.3c02719
ACS Omega 2023, 8, 27355−27365

of redox-active molecules to facilitate the cross-membrane transport of electrons. Tunneling distance and redox potentials (reaction Gibbs energy) of cofactors are viewed as main physical parameters of this design.[27,28] The protein identity, flexibility, or dynamics are missing from this picture, assigning universal charge-transport properties to all proteins. Dynamic models of electron transfer challenge this paradigm. Computer simulations of protein electron transfer show that the hopping rate must stay constant at $R < R^* \simeq 11-12$ Å. The standard exponential falloff of the rate is restored at $R > R^*$. Energy chains for electron transport are best designed by placing the redox cofactors near the crossover distance R^*. Protein flexibility and dynamics affect the magnitude of the maximum hopping rate within the crossover distance. Vectorial (unidirectional) transport of electrons is driven by both thermodynamics (barrier height) and dynamics/flexibility (crossover parameter g).

■ ASSOCIATED CONTENT

Supporting Information

The Supporting Information is available free of charge at https://pubs.acs.org/doi/10.1021/acsomega.3c02719.

Simulation protocols, atomic charges from quantum calculations, protocols for applying the Q-model, and calculations of donor−acceptor electronic coupling (PDF)

■ AUTHOR INFORMATION

Corresponding Author

Dmitry V. Matyushov − *School of Molecular Sciences and Department of Physics, Arizona State University, Tempe, Arizona 85287-1504, United States;* orcid.org/0000-0002-9352-764X; Phone: (480)965-0057; Email: dmitrym@asu.edu

Author

Setare Mostajabi Sarhangi − *School of Molecular Sciences and Department of Physics, Arizona State University, Tempe, Arizona 85287-1504, United States*

Complete contact information is available at: https://pubs.acs.org/10.1021/acsomega.3c02719

Notes

The authors declare no competing financial interest.

■ ACKNOWLEDGMENTS

This research was supported by the National Science Foundation (CHE-2154465). The supercomputer time was provided through Extreme Science and Engineering Discovery Environment (XSEDE) allocation MCB080071 and through ASU's Research Computing. We are grateful to Matthew Guberman-Pfeffer for discussions and help in performing electronic coupling calculations.

■ REFERENCES

(1) de Vault, D.; Chance, B. Studies of phosynthesis using a pulsed laser. I. Temperature dependence of cytochrome oxidation rate in Chromatium. Evidence for tunneling. *Biophys. J.* **1966**, *6*, 825.

(2) DeVault, D. *Quantum-Mechanical Tunneling in Biologycal Systems*; Cambridge University Press: Cambridge, UK, 1984.

(3) Mitchell, P. Coupling of Phosphorylation to Electron and Hydrogen Transfer by a Chemi-Osmotic type of Mechanism. *Nature* **1961**, *191*, 144−148.

(4) Nicholls, D. G.; Ferguson, S. J. *Bioenergetics 4*; Academic Press: Amsterdam, 2013.

(5) Szent-Gyorgyi, A. The study of energy levels in biochemistry. *Nature* **1941**, *148*, 157−159.

(6) Pethig, R.; Szent-Györgyi, A. Electronic properties of the casein-methylglyoxal complex. *Proc. Natl. Acad. Sci. U. S. A.* **1977**, *74*, 226−228.

(7) McGinness, J.; Corry, P.; Proctor, P. Amorphous Semiconductor Switching in Melanins. *Science* **1974**, *183*, 853−855.

(8) Barbara, P. F.; Olson, E. J. C. Experimental electron transfer kinetics in a DNA environment. *Adv. Chem. Phys.* **2016**, *107*, 647−676.

(9) Beratan, D. N.; Liu, C.; Migliore, A.; Polizzi, N. F.; Skourtis, S. S.; Zhang, P.; Zhang, Y. Charge transfer in dynamical biosystems, or the treachery of (static) images. *Acc. Chem. Res.* **2015**, *48*, 474−481.

(10) Bostick, C. D.; Mukhopadhyay, S.; Pecht, I.; Sheves, M.; Cahen, D.; Lederman, D. Protein bioelectronics: a review of what we do and do not know. *Rep. Prog. Phys.* **2018**, *81*, 026601.

(11) Moser, C. C.; Keske, J. M.; Warncke, K.; Farid, R. S.; Dutton, P. L. Nature of biological electron transfer. *Nature* **1992**, *355*, 796−802.

(12) Gray, H. B.; Winkler, J. R. Long-range electron transfer. *Proc. Natl. Acad. Sci. U. S. A.* **2005**, *102*, 3534−3539.

(13) Lovley, D. R.; Walker, D. J. F. Geobacter Protein Nanowires. *Frontiers in Microbiology* **2019**, *10*, 2078.

(14) Wang, F.; Gu, Y.; O'Brien, J. P.; Yi, S. M.; Yalcin, S. E.; Srikanth, V.; Shen, C.; Vu, D.; Ing, N. L.; Hochbaum, A. I.; et al. Structure of microbial nanowires reveals stacked hemes that transport electrons over micrometers. *Cell* **2019**, *177*, 361−369.e10.

(15) Giese, B.; Graber, M.; Cordes, M. Electron transfer in peptides and proteins. *Curr. Opin. Chem. Biol.* **2008**, *12*, 755−759.

(16) Shipps, C.; Kelly, H. R.; Dahl, P. J.; Yi, S. M.; Vu, D.; Boyer, D.; Glynn, C.; Sawaya, M. R.; Eisenberg, D.; Batista, V. S.; et al. Intrinsic electronic conductivity of individual atomically resolved amyloid crystals reveals micrometer-long hole hopping via tyrosines. *Proc. Natl. Acad. Sci. U.S.A.* **2021**, *118*, No. e2014139118.

(17) Dahl, P. J.; Yi, S. M.; Gu, Y.; Acharya, A.; Shipps, C.; Neu, J.; O'Brien, J. P.; Morzan, U. N.; Chaudhuri, S.; Guberman-Pfeffer, M. J.; et al. A 300-fold conductivity increase in microbial cytochrome nanowires due to temperature-induced restructuring of hydrogen bonding networks. *Sci. Adv.* **2022**, *8*, No. eabm7193.

(18) Gamow, G. Zur Quantentheorie des Atomkernes. *Z. Phys.* **1928**, *51*, 204−212.

(19) Moser, C. C.; Chobot, S. E.; Page, C. C.; Dutton, P. L. Distance metrics for heme protein electron tunneling. *Biochim. Biophys. Acta - Bioenergetics* **2008**, *1777*, 1032−1037.

(20) Lax, M. The Frank-Condon principle and its application to crystals. *J. Chem. Phys.* **1952**, *20*, 1752−1760.

(21) Landau, L. D.; Lifshits, E. M. *Quantum Mechanics: Non-Relativistic Theory*; Pergamon Press: Oxford, 1977.

(22) Hoff, A. J.; Deisenhofer, J. Photophysics of photosynthesis. *Phys. Rep.* **1997**, *287*, 1−247.

(23) Warshel, A. Dynamics of reactions in polar solvents. Semiclassical trajectory studies of electron-transfer and proton-transfer reactions. *J. Phys. Chem.* **1982**, *86*, 2218−2224.

(24) Skourtis, S. S.; Waldeck, D. H.; Beratan, D. N. Fluctuations in biological and bioinspired electron-transfer reactions. *Annu. Rev. Phys. Chem.* **2010**, *61*, 461−485.

(25) Winkler, J. R.; Gray, H. B. Electron flow through metalloproteins. *Chem. Rev.* **2014**, *114*, 3369−3380.

(26) Gray, H. B.; Winkler, J. R. Functional and protective hole hopping in metalloenzymes. *Chem. Sci.* **2021**, *12*, 13988−14003.

(27) Page, C. C.; Moser, C. C.; Chen, X. X.; Dutton, P. L. Natural engineering principles of electron tunneling in biological oxidation-reduction. *Nature* **1999**, *402*, 47−52.

(28) Moser, C. C.; Anderson, J. R.; Dutton, P. L. Guidelines for tunneling in enzymes. *Biochim. Biophys. Acta - Bioenergetics* **2010**, *1797*, 1573−1586.

(29) Marcus, R. A.; Sutin, N. Electron transfer in chemistry and biology. *Biochim. Biophys. Acta* **1985**, *811*, 265−322.

(30) Choi, S. H.; Kim, B.; Frisbie, C. D. Electrical resistance of long conjugated molecular wires. *Science* **2008**, *320*, 1482−1486.
(31) Pauling, L. Molecular architecture and biological reactions. *Chem. Eng. News* **1946**, *24*, 1375−1377.
(32) Klinman, J. P.; Kohen, A. Hydrogen tunneling links protein dynamics to enzyme catalysis. *Annu. Rev. Biochem.* **2013**, *82*, 471−496.
(33) Kern, D.; Zuiderweg, E. R. P. The role of dynamics in allosteric regulation. *Curr. Opin. Struct. Biol.* **2003**, *13*, 748−757.
(34) Henzler-Wildman, K. A.; Thai, V.; Lei, M.; Ott, M.; Wolf-Watz, M.; Fenn, T.; Pozharski, E.; Wilson, M. A.; Petsko, G. A.; Karplus, M.; et al. Intrinsic motions along an enzymatic reaction trajectory. *Nature* **2007**, *450*, 838−844.
(35) Kohen, A. Role of Dynamics in Enzyme Catalysis: Substantial versus Semantic Controversies. *Acc. Chem. Res.* **2015**, *48*, 466−473.
(36) Finklea, H. O. Electrochemistry of organized monolayers of thiols and related molecules on electrodes. *Electroanal. Chem.: A series of advances* **1996**, *19*, 109−335.
(37) Murgida, D. H.; Hildebrandt, P. Redox and redox-coupled processes of heme proteins and enzymes at electrochemical interfaces. *Phys. Chem. Chem. Phys.* **2005**, *7*, 3773−3784.
(38) Waldeck, D. H.; Khoshtariya, D. E. *Applications of Electrochemistry and Nanotechnology in Biology and Medicine I*; Springer: New York: New York, NY, 2011; pp 105−238.
(39) Alvarez-Paggi, D.; Hannibal, L.; Castro, M. A.; Oviedo-Rouco, S.; Demicheli, V.; Tórtora, V.; Tomasina, F.; Radi, R.; Murgida, D. H. Multifunctional cytochrome c: Learning new tricks from an old dog. *Chem. Rev.* **2017**, *117*, 13382−13460.
(40) Buhrke, D.; Hildebrandt, P. Probing structure and reaction dynamics of proteins using time-resolved resonance Raman spectroscopy. *Chem. Rev.* **2020**, *120*, 3577−3630.
(41) Murgida, D. H.; Hildebrandt, P. Proton-coupled electron transfer of cytochrome c. *J. Am. Chem. Soc.* **2001**, *123*, 4062−4068.
(42) Chi, Q.; Zhang, J.; Andersen, J. E. T.; Ulstrup, J. Ordered assembly and controlled electron transfer of the blue copper protein azurin at gold (111) single-crystal substrates. *J. Phys. Chem. B* **2001**, *105*, 4669−4679.
(43) Wei, J. J.; Liu, H.; Niki, K.; Margoliash, E.; Waldeck, D. H. Probing electron tunneling pathways: Electrochemical study of rat heart cytochrome *c* and its mutant on pyridine-terminated SAMs. *J. Phys. Chem. B* **2004**, *108*, 16912−16917.
(44) Zitare, U. A.; Szuster, J.; Santalla, M. C.; Morgada, M. N.; Vila, A. J.; Murgida, D. H. Dynamical effects in metalloprotein heterogeneous electron transfer. *Electrochim. Acta* **2020**, *342*, 136095.
(45) Alvarez-Paggi, D.; Zitare, U.; Murgida, D. H. The role of protein dynamics and thermal fluctuations in regulating cytochrome c/cytochrome c oxidase electron transfer. *Biochim. Biophys. Acta - Bioenergetics* **2014**, *1837*, 1196−1207.
(46) Zusman, L. D. Outer-sphere electron transfer in polar solvents. *Chem. Phys.* **1980**, *49*, 295−304.
(47) Sumi, H.; Marcus, R. A. Dynamical effects in electron transfer reactions. *J. Chem. Phys.* **1986**, *84*, 4894−4914.
(48) Hynes, J. T. Outer-sphere electron-transfer reactions and frequency-dependent friction. *J. Phys. Chem.* **1986**, *90*, 3701−3706.
(49) Rips, I.; Jortner, J. Dynamic solvent effects on outer-sphere electron transfer. *J. Chem. Phys.* **1987**, *87*, 2090−2104.
(50) Yan, Y. J.; Sparpaglione, M.; Mukamel, S. Solvation dynamics in electron-transfer, isomerization, and nonlinear optical processes: a unified Liouville-space theory. *J. Phys. Chem.* **1988**, *92*, 4842−4853.
(51) van der Zwan, G.; Hynes, J. T. Time-dependent fluorescence solvent shifts, dielectric friction, and nonequilibrium solvation in polar solvents. *J. Phys. Chem.* **1985**, *89*, 4181−4188.
(52) Maroncelli, M. The dynamics of solvation in polar liquids. *J. Mol. Liq.* **1993**, *57*, 1−37.
(53) Kramers, H. Brownian motion in a field of force and the diffusion model of chemical reactions. *Physica* **1940**, *7*, 284−304.
(54) Frauenfelder, H.; Wolynes, P. G. Rate theories and puzzles of hemeprotein kinetics. *Science* **1985**, *229*, 337−345.
(55) Hänggi, P.; Talkner, P.; Borkovec, M. Reaction-rate theory: fifty years after Kramers. *Rev. Mod. Phys.* **1990**, *62*, 251−341.
(56) Jimenez, R.; Fleming, G. R.; Kumar, P. V.; Maroncelli, M. Femtosecond solvation dynamics of water. *Nature* **1994**, *369*, 471−473.
(57) Seyedi, S.; Waskasi, M. M.; Matyushov, D. V. Theory and electrochemistry of cytochrome *c*. *J. Phys. Chem. B* **2017**, *121*, 4958−4967.
(58) Matyushov, D. V. Dynamical effects in protein electrochemistry. *J. Phys. Chem. B* **2019**, *123*, 7290−7301.
(59) Page, C. C.; Moser, C. C.; Dutton, P. L. Mechanism for electron transfer within and between proteins. *Curr. Opinion in Biology* **2003**, *7*, 551.
(60) Sarhangi, S. M.; Matyushov, D. V. Theory of protein charge transfer: Electron transfer between tryptophan residue and active site of azurin. *J. Phys. Chem. B* **2022**, *126*, 10360−10373.
(61) Shih, C.; Museth, A. K.; Abrahamsson, M.; Blanco-Rodriguez, A. M.; Di Bilio, A. J.; Sudhamsu, J.; Crane, B. R.; Ronayne, K. L.; Towrie, M.; Vlček, A.; et al. Tryptophan-accelerated electron flow through proteins. *Science* **2008**, *320*, 1760−1762.
(62) Matyushov, D. V. Conformational dynamics modulating electron transfer. *J. Chem. Phys.* **2022**, *157*, 095102.
(63) Hoganson, C. W.; Tommos, C. The function and characteristics of tyrosyl radical cofactors. *Biochim. Biophys. Acta - Bioenergetics* **2004**, *1655*, 116−122.
(64) LeBard, D. N.; Matyushov, D. V. Protein-water electrostatics and principles of bioenergetics. *Phys. Chem. Chem. Phys.* **2010**, *12*, 15335−15348.
(65) Matyushov, D. V.; Voth, G. A. Modeling the free energy surfaces of electron transfer in condensed phases. *J. Chem. Phys.* **2000**, *113*, 5413−5424.
(66) Garner, D. K.; Vaughan, M. D.; Hwang, H. J.; Savelieff, M. G.; Berry, S. M.; Honek, J. F.; Lu, Y. Reduction potential tuning of the blue copper center in Pseudomonas Aeruginosa azurin by the axial methionine as probed by unnatural amino acids. *J. Am. Chem. Soc.* **2006**, *128*, 15608−15617.
(67) Tommos, C.; Babcock, G. T. Proton and hydrogen currents in photosynthetic water oxidation. *Biochim. Biophys. Acta - Bioenergetics* **2000**, *1458*, 199−219.
(68) Tachiya, M. Relation between the electron-transfer rate and the free energy change of reaction. *J. Phys. Chem.* **1989**, *93*, 7050−7052.
(69) Small, D. W.; Matyushov, D. V.; Voth, G. A. The theory of electron transfer: What may be missing? *J. Am. Chem. Soc.* **2003**, *125*, 7470−7478.
(70) Blumberger, J. Free energies for biological electron transfer from QM/MM calculation: method, application and critical assessment. *Phys. Chem. Chem. Phys.* **2008**, *10*, 5651−5667.
(71) Matyushov, D. V. Protein electron transfer: is biology (thermo)dynamic? *J. Phys.: Condens. Matter* **2015**, *27*, 473001.
(72) Allen, M. P.; Tildesley, D. J. *Computer Simulation of Liquids*; Clarendon Press: Oxford, 1996.
(73) Kuharski, R. A.; Bader, J. S.; Chandler, D.; Sprik, M.; Klein, M. L.; Impey, R. W. Molecular model for aqueous ferrous-ferric electron transfer. *J. Chem. Phys.* **1988**, *89*, 3248−3257.
(74) Voityuk, A. A. Electron transfer between [4Fe−4S] clusters. *Chem. Phys. Lett.* **2010**, *495*, 131−134.
(75) Consani, C.; Aubock, G.; van Mourik, F.; Chergui, M. Ultrafast tryptophan-to-heme electron transfer in myoglobins revealed by UV 2D spectroscopy. *Science* **2013**, *339*, 1586−1589.
(76) Lüdemann, G.; Woiczikowski, P. B.; Kubař, T.; Elstner, M.; Steinbrecher, T. B. Charge Transfer in E. coli DNA Photolyase: Understanding Polarization and Stabilization Effects via QM/MM Simulations. *J. Phys. Chem. B* **2013**, *117*, 10769−10778.
(77) Cailliez, F.; Müller, P.; Firmino, T.; Pernot, P.; de la Lande, A. Energetics of photoinduced charge migration within the tryptophan tetrad of an animal (6−4) photolyase. *J. Am. Chem. Soc.* **2016**, *138*, 1904−1915.
(78) Jiang, X.; van Wonderen, J. H.; Butt, J. N.; Edwards, M. J.; Clarke, T. A.; Blumberger, J. Which multi-heme protein complex

https://doi.org/10.1021/acsomega.3c02719
ACS Omega 2023, 8, 27355−27365

transfers electrons more efficiently? Comparing MtrCAB from shewanella with OmcS from geobacter. *J. Phys. Chem. Lett.* **2020**, *11*, 9421−9425.
(79) Polizzi, N. F.; Migliore, A.; Therien, M. J.; Beratan, D. N. Defusing redox bombs? *Proc. Natl. Acad. Sci. U.S.A.* **2015**, *112*, 10821−10822.
(80) Guberman-Pfeffer, M. J. Assessing thermal response of redox conduction for nti-Arrhenius kinetics in a microbial cytochrome nanowire. *J. Phys. Chem. B* **2022**, *126*, 10083−10097.
(81) Záliš, S.; Heyda, J.; Šebesta, F.; Winkler, J. R.; Gray, H. B.; Vlček, A. Photoinduced hole hopping through tryptophans in proteins. *Proc. Natl. Acad. Sci. U.S.A.* **2021**, *118*, No. e2024627118.
(82) Frauenfelder, H.; Sligar, S. G.; Wolynes, P. G. The energy landscapes and motions of proteins. *Science* **1991**, *254*, 1598−1603.
(83) Skov, L. K.; Pascher, T.; Winkler, J. R.; Gray, H. B. Rates of intramolecular electron transfer in $Ru(bpy)_2(im)$(His83)-modified azurin increase below 220 K. *J. Am. Chem. Soc.* **1998**, *120*, 1102−1103.
(84) Kayser, B.; Fereiro, J. A.; Bhattacharyya, R.; Cohen, S. R.; Vilan, A.; Pecht, I.; Sheves, M.; Cahen, D. Solid-state electron transport via the protein azurin is temperature-independent down to 4 K. *J. Phys. Chem. Lett.* **2020**, *11*, 144−151.
(85) Amdursky, N.; Sepunaru, L.; Raichlin, S.; Pecht, I.; Sheves, M.; Cahen, D. Electron transfer proteins as electronic conductors: Significance of the metal and its binding site in the blue Cu protein, azurin. *Adv. Sci.* **2015**, *2*, 1400026.
(86) Valianti, S.; Cuevas, J.-C.; Skourtis, S. S. Charge-transport mechanisms in azurin-based monolayer junctions. *J. Phys. Chem. C* **2019**, *123*, 5907−5922.
(87) Stubbe, J.; Nocera, D. G.; Yee, C. S.; Chang, M. C. Y. Radical initiation in the class I ribonucleotide reductase: Long-range proton-coupled electron transfer? *Chem. Rev.* **2003**, *103*, 2167−2202.
(88) Bollinger, M. J. Electron relay in proteins. *Science* **2008**, *320*, 1730−1731.
(89) Zhang, B.; Ryan, E.; Wang, X.; Song, W.; Lindsay, S. Electronic transport in molecular wires of precisely controlled length built from modular proteins. *ACS Nano* **2022**, *16*, 1671−1680.
(90) Nagel, Z. D.; Klinman, J. P. Tunneling and dynamics in enzymatic hydride transfer. *Chem. Rev.* **2006**, *106*, 3095−3118.
(91) Amdursky, N.; Pecht, I.; Sheves, M.; Cahen, D. Marked changes in electron transport through the blue copper protein azurin in the solid state upon deuteration. *Proc. Natl. Acad. Sci. U.S.A.* **2013**, *110*, 507−512.
(92) Mostajabi Sarhangi, S.; Matyushov, D. V. Effect of water deuteration on protein electron transfer. *J. Phys. Chem. Lett.* **2023**, *14*, 723−729.
(93) Dinpajooh, M.; Newton, M. D.; Matyushov, D. V. Free energy functionals for polarization fluctuations: Pekar factor revisited. *J. Chem. Phys.* **2017**, *146*, 064504.
(94) Matyushov, D. V. Reorganization energy of electron transfer. *Phys. Chem. Chem. Phys.* **2023**, *25*, 7589−7610.
(95) Hopfield, J. J. Electron Transfer Between Biological Molecules by Thermally Activated Tunneling. *Proc. Natl. Acad. Sci. U.S.A.* **1974**, *71*, 3640−3644.
(96) Jortner, J. Temperature dependent activation energy for electron transfer between biological molecules. *J. Chem. Phys.* **1976**, *64*, 4860−4867.
(97) Jortner, J.; Ulstrup, J. Dynamics of nonadiabatic atom transfer in biological systems. Carbon monoxide binding to hemoglobin. *J. Am. Chem. Soc.* **1979**, *101*, 3744−3754.
(98) Alberding, N.; Austin, R. H.; Beeson, K. W.; Chan, S. S.; Eisenstein, L.; Frauenfelder, H.; Nordlund, T. M. Tunneling in ligand binding to heme proteins. *Science* **1976**, *192*, 1002−1004.
(99) Frauenfelder, H. In *Tunneling in Biological Systems*; Chance, B., DeVault, D., Frauenfelder, H., Marcus, R. A., Schrieffer, J. R., Sutin, N., Eds.; Academic Press: New York, 1979; pp 627−649.
(100) Szent-Györgyi, A. *Bioelectronics. A Study in Cellular Regulations, Defense, and Cancer*; Academic Press: New York, NY, 1968.
(101) Landauer, R.; Martin, T. Barrier interaction time in tunneling. *Rev. Mod. Phys.* **1994**, *66*, 217−228.
(102) Lovley, D. R. Electrically conductive pili: Biological function and potential applications in electronics. *Curr. Opin. Electrochem.* **2017**, *4*, 190−198.
(103) Yalcin, S. E.; Malvankar, N. S. The blind men and the filament: Understanding structures and functions of microbial nanowires. *Cur. Opin. Chem. Biol.* **2020**, *59*, 193−201.
(104) Warren, J. J.; Gray, H. B. *In Comprehensive Coordination Chemistry III*; Constable, E. C., Parkin, G., Que, Jr, L., Eds.; Elsevier: Oxford, 2021; Vol. *8*; pp 3−18.
(105) Gray, H. B.; Winkler, J. R. Electron tunneling through proteins. *Q. Rev. Biophys.* **2003**, *36*, 341−372.

https://doi.org/10.1021/acsomega.3c02719
ACS Omega 2023, 8, 27355−27365